Population dynamics, information transfer, and spatial organization in a chemical reaction network under spatial confinement and crowding conditions

Giovanni Bellesia*
Theoretical Biology and Biophysics Group, Los Alamos National Laboratory, Los Alamos, New Mexico 87545, USA

Benjamin B. Bales
Department of Computer Science, University of California Santa Barbara, Santa Barbara, California 93106, USA
(Received 21 May 2016; revised manuscript received 24 July 2016; published 10 October 2016)

We investigate, via Brownian dynamics simulations, the reaction dynamics of a generic, nonlinear chemical network under spatial confinement and crowding conditions. In detail, the Willamowski-Rossler chemical reaction system has been "extended" and considered as a prototype reaction-diffusion system. Our results are potentially relevant to a number of open problems in biophysics and biochemistry, such as the synthesis of primitive cellular units (protocells) and the definition of their role in the chemical origin of life and the characterization of vesicle-mediated drug delivery processes. More generally, the computational approach presented in this work makes the case for the use of spatial stochastic simulation methods for the study of biochemical networks *in vivo* where the "well-mixed" approximation is invalid and both thermal and intrinsic fluctuations linked to the possible presence of molecular species in low number copies cannot be averaged out.

DOI: 10.1103/PhysRevE.94.042306

I. INTRODUCTION

Biochemical networks *in vivo* are typically *open* to the exchange of energy and matter with the surrounding environment [1–4]. They often contain autocatalytic steps [5–9] and their dynamics tends to be strongly influenced by thermal and intrinsic noise [10,11], macromolecular crowding, and spatial confinement [12–18]. In this study we investigate by means of an extended set of Brownian dynamics simulations how the dynamics of a generic chemical network is affected by spatial confinement and particle crowding [12,13,16–18]. The reaction-diffusion system considered in this study is based on the Willamowski-Rossler (WR) chemical network [19] [see Fig. 1(a)]; a nonlinear, continuous-time minimal model for chemical chaos based on first- and second-order chemical reactions. The WR network contains three autocatalytic steps involving species A, B, and C and is thermodynamically open [1–4]. The rate equations defining the original implementation of the model [19] display a rich and complicated dynamics comprising fixed point, limit cycle, and chaotic attractors. The WR network has been previously studied via deterministic and nonspatial stochastic simulation methods [20–25] but never as a stochastic reaction-diffusion system where crowding and spatial confinement are explicitly taken into account.

In this study we investigate the effects of spatial confinement and crowding on a *minimal* version of the WR network (MWR) (see Fig. 1(b) and Ref. [25]) using hard-sphere [26,27] Brownian dynamics simulations integrating chemical reactivity [28,29]. We fix the population numbers for species E_1, E_2, E_3, P_1, and P_2 (consequently the rates k_1, k_3, and k_5 become pseudo-first-order) to make the chemical network thermodynamically open. The following chemical reactions describe the MWR system used in our simulations [25] [see also Fig. 1(a)]:

$$\bar{E}_1 + A \underset{k_{-1}}{\overset{k_1}{\rightleftharpoons}} 2A, \tag{1a}$$

$$A + B \xrightarrow{k_2} 2B, \tag{1b}$$

$$A + C \xrightarrow{k_4} \not{P}_2, \tag{1c}$$

$$\bar{E}_2 + B \xrightarrow{k_3} \not{P}_1, \tag{1d}$$

$$\bar{E}_3 + C \underset{k_{-5}}{\overset{k_5}{\rightleftharpoons}} 2C. \tag{1e}$$

The main assumption in the MWR system [19,25] is that three of the backward reaction rate constants shown in Fig. 1(a), namely k_{-2}, k_{-3}, and k_{-4}, are much smaller than their forward counterparts and, hence, can be neglected. The MWR system is composed of two main subsystems: a Lotka-Volterra oscillator [30–32] involving species A and B and a chemical *switch* [20] that couples the Lotka-Volterra component to species C through species A.

Similarly to the "full" WR network, the MWR rate equations derived from the set of chemical reactions (1a)–(1e) display a diverse dynamical behavior comprising fixed point, limit cycle, and chaotic attractors [19,25].

We employ various information theory (IT) functionals and (spectral) graph theory to quantify the effects of confinement and crowding on the population dynamics, transfer of information, and spatial organization within the MWR network. Our results show that while the effects of a variable container volume are overall linear, the influence of a variable number of crowders is not immediately quantifiable in a simple analytical way and translates differently to the three different species in the MWR network. Our analysis reveals a number of relevant details about the dynamical nature of the MWR network that are not accessible to simpler models which do not

*giovanni.bellesia@gmail.com

consider excluded volume effects, spatial inhomogeneity, and the particle nature of the chemical system under consideration.

We believe that modeling techniques based on Brownian dynamics simulations integrating chemical reactivity could be, for example, particularly appealing in the theoretical and computational study of primitive cellular units or protocells; their synthesis, their stationary dynamics, and their role in the chemical origin of life [4,8,9,33–41]. Another possible application for "reactive" Brownian models relates to the study of gene regulatory networks and in particular of synchronized genetic oscillators [42–45] where chemical species responsible for both the activation and the repression of gene activity diffuse between neighboring cells and interact with specific receptors on their surface.

More generally, we make the case for a more widespread development and use of spatial stochastic simulation methods of biochemical networks *in vivo* that explicitly take into account confinement and macromolecular crowding [12,46–53].

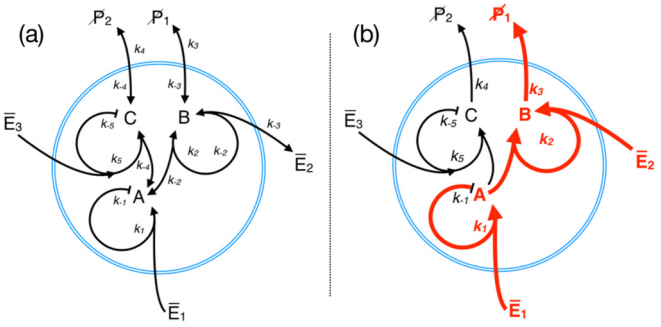

FIG. 1. Schematic view of the Willamowski-Rossler chemical network. (a) The *full* version. (b) The *minimal* version analyzed in this study obtained by setting $k_{-2} = k_{-3} = k_{-4} = 0$. In red we highlight the Lotka-Volterra component of the network [19,25]. The overbar on species E_1, E_2, and E_3 indicates that the concentrations of those species are constants and the diagonal segment crossing P_1 and P_2 indicates that those species are instantaneously eliminated from the system (see Sec. II for details).

II. METHODS

All three autocatalytic species A, B, and C are spatially confined within a spherical *container*, E_1 and E_3 catalyze the synthesis of A and C, respectively, whereas E_2 catalyzes the degradation of B. P_1 and P_2 are the products of reactions (1d) and (1c), respectively, and they get instantaneously eliminated from the reaction pool, i.e., their constant population number is zero. The constant population numbers of E_1, E_2, and E_3 and the instantaneous elimination of P_1 and P_2 lead to a biochemical network composed of A, B, and C which is spatially enclosed and thermodynamically open, i.e., it exchanges matter and energy with the surrounding environment by means of three *sources* (E_1, E_2, and E_3) and two *sinks* (P_1 and P_2). The constant values of E_1, E_2, E_3 are incorporated into the *pseudo*-first-order rates k_1, k_3, k_5, respectively (see Fig. 1).

The different chemical species in the MWR system are modeled as *reactive*, Brownian hard spheres confined in a spherical, *hard* container. The details of the Brownian integra-

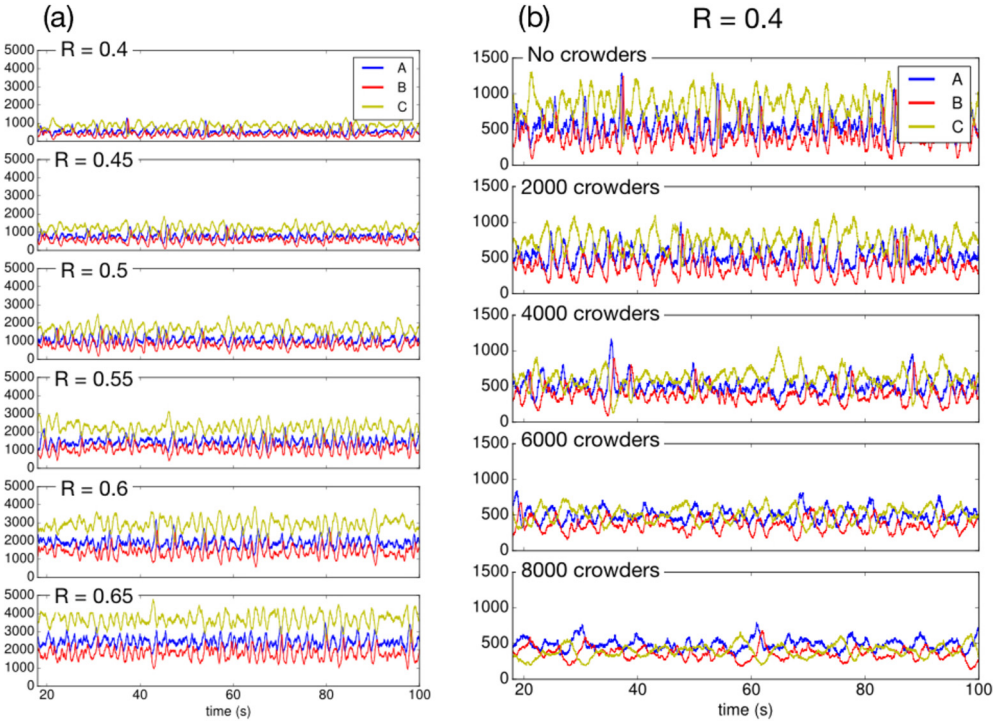

FIG. 2. Population time series (partial time windows) obtained each from a single trajectory of our Brownian dynamics simulations of the MWR network with *kset3* parametrization. (a) Population time series for systems with varying volume (radii varying from 0.4 to 0.65 μm). (b) Population time series for systems with varying number of crowders and with constant container volume. The radius of the spherical container is $R = 0.4$ μm.

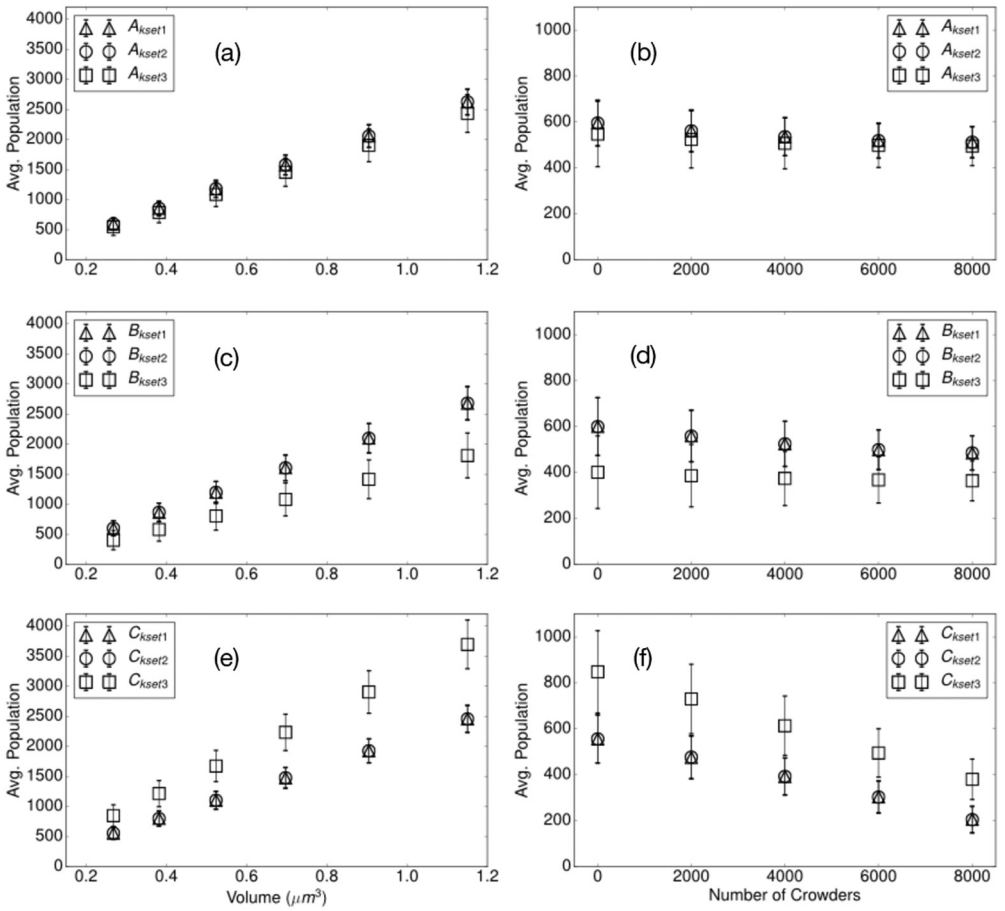

FIG. 3. Average population values for species A [(a) and (b)], B [(c) and (d)], and C [(e) and (f)] with parametrizations *kset1*, *kset2*, and *kset3*. (a), (c), and (e) The average populations are plotted against the volume of the spherical container, no inert crowders are present. The average population of the reactive species grows linearly with the volume of the spherical container. (b), (d), and (f) The average populations are plotted against the number of inert crowders. A slight decrease in the average population is observed when the number of inert crowders within a spherical container of radius $R = 0.4$ μm is increased from 0 to 8000. The presence of the inert crowders affects differently the three chemical species in the MWR network.

tor used in our simulations can be found in Refs. [28,29]. The radius of the hard spheres for species A, B, and C is 0.01 μm and the diffusion coefficient is $D = 0.01$ $\mu\text{m}^2\,\text{s}^{-1}$. In all our simulations the time step is fixed at $\Delta t = 0.01$ s.

To study the effects of crowding and confinement we run two separate sets of reactive Brownian dynamics simulations. In the first set we consider six different spherical containers with radius varying between 0.4 and 0.65 μm. The containers are implemented as "hard-wall" spherical boundary conditions. For each of the six spherical containers we run a total of 30 independent simulations, each of total time $t_{\text{tot}} = 1000$ s. Three sets of values for the reaction rate constants (*kset1*, *kset2*, *kset3*) are used for each one of the six different spherical containers. They correspond to three distinct dynamical behaviors in the deterministic implementation of the MWR model: fixed point, limit cycle, and chaotic dynamics, respectively. The first set (*kset1*, fixed point attractor) is $k_1 = 30.0$, $k_{-1} = 0.25$, $k_2 = 1.0$, $k_3 = 10.0$, $k_4 = 0.4$, $k_5 = 16.5$, and $k_{-5} = 0.5$. To generate the second set (*kset2*, limit cycle attractor) we simply consider the first set of parameters and change the value of k_4 to 0.6. In the third set (*kset3*, chaotic attractor) we set $k_4 = 0.6$, $k_5 = 18.5$, and $k_{-5} = 0.4$. In other words, *kset2* is generated from *kset1* by increasing the degradation of A and C (increasing the coupling between the Lotka-Volterra component and the *switch*) while *kset3* is obtained from *kset1* by increasing both the A-C coupling and decreasing the ratio k_{-5}/k_5.

We run ten independent simulations for each of the three parameter sets. The starting point for each simulation is generated randomly placing $A = B = C = 100$ hard spheres within the proper spherical container. In the second set of simulations we take into account the presence of a variable number of "chemically inert" crowders modeled as hard spheres of radius $r = 0.01$ μm and with diffusion coefficient $D = 0.01$ $\mu\text{m}^2\,\text{s}^{-1}$. The starting point for each simulation in the second set is generated randomly placing $A = B = C = 100$ hard spheres and a variable number of inert crowders, with same radius and diffusion coefficient as A, B, and C in a spherical container with radius $R = 0.4$ μm. We run independent simulations for five different crowder population numbers: varying between 2×10^3 and 8×10^3. For each of the five crowder population numbers we run a total of 30 independent simulations (ten for each of the three parameters sets), each of total time $t_{\text{tot}} = 1000$ s.

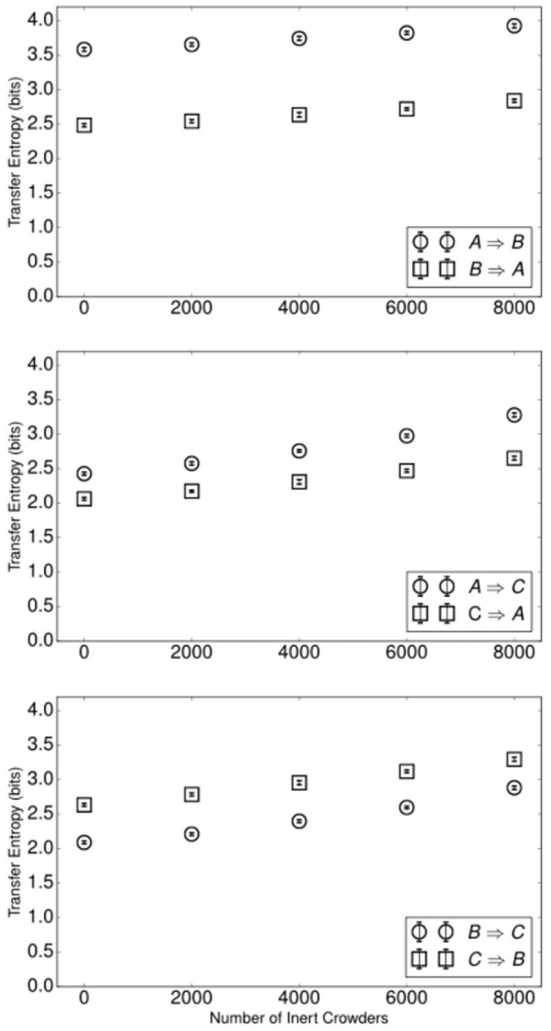

FIG. 4. Transfer entropy as a function of the number of inert crowders (constant container volume). Data refer to *kset3* parametrization.

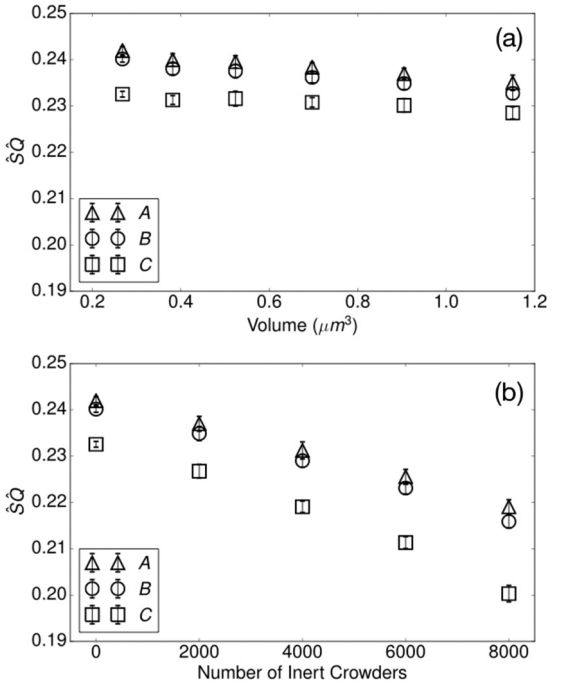

FIG. 5. (a) Statistical complexity measure as a function of the container volume with no inert crowders present. (b) Statistical complexity measure as a function of the number of inert crowders at constant container volume. Data refer to *kset3* parametrization.

III. RESULTS AND DISCUSSION

A. Population dynamics

We focus our analysis on the stationary [54] portion of our Brownian dynamics simulations. In Fig. 2 we show a set of representative time windows for the population numbers of species A, B, and C related to simulations with variable container volume and no inert crowders present [Fig. 1(a)], and to simulations with container radius $R = 0.4$ μm and varying number of inert crowders from 0 to 8000 [Fig. 1(b)]. All data refer to parametrization *kset3*. Time series population data generated under *kset1* and *kset2* are not shown as they display similar temporal patterns. Figure 2 qualitatively shows that (1) both average population and fluctuations increase with increasing container volume for all species and (2) the presence of an increasing number of inert crowders affects the average population of species A, B, and C in different, nontrivial ways. The presence of an increasing number of inert crowders also appears to lower both the magnitude of the fluctuations in the population dynamics and the temporal interdependence between the populations of the different species. A quantitative assessment of the mean and fluctuations dependence from both the container volume and the crowders number is given in Fig. 3. In Fig. 3(a) we show that in the limited range of container volumes considered in our simulations, the mean population increases linearly with increasing container volume. The fluctuations calculated as the standard deviation from the mean also have a tendency to increase although not linearly. The effects of the presence of inert crowders are shown in the Fig. 3(b). A, B, and C "chemical" species all show a decrease in their average population for increasing crowder numbers which can be intuitively related to the diminished availability of free volume within the spherical container. The decrease is more apparent, and linear in nature, for species C (bottom right) than it is for A and B which both appear to reach a plateau as the number of crowders increases. It is worth pointing out how, even in a simple chemical network like the MWR network, the effects of crowding are far from being uniform across the different chemical species and cannot be easily incorporated in lower-resolution reaction-diffusion models that do not explicitly consider excluded volume effects and spatial granularity. An additional observation on the data in Fig. 3 which is more specific to the MWR chemical network relates to the dependence of the average population from the parametrization set. First, the population dynamics of species A, B, and C does not change significantly when the parametrization set changes from *kset1* to *kset2*. Second, the transition from parametrization *kset1* and *kset2* to *kset3* has opposite effects on species B and C. Third, species A does not show any quantifiable dependence from the parameter set (under both volume and crowders' number varying conditions). It is easy to connect the increase in the slope of the average population of species C to the increase in C's net synthesis

going from *kset1* and *kset2* to *kset3*. The decrease in the linear fit's slope for species B is less clear since species B is not directly affected by the changes in the parametrization set and species A, which is directly coupled to B, is insensitive to those changes. The low sensitivity to parameter changes of species A can be qualitatively explained considering that A is the connection point in the MWR network between the Lotka-Volterra component and the *switch* component [20] and therefore might benefit from the mutual "modulation" given by species B and C. The results on the population dynamics shown in Fig. 3 and discussed in this section are an example of the level of detail that can be attained only with particle-based, spatial stochastic models. Indeed, the presence of excluded volume effects and the explicit representation of the reactor volume and its boundaries set the Brownian simulator apart from both the deterministic and the stochastic well-mixed simulators. All three dynamic regimes (fixed point, limit cycle, chaotic) generated under parametrizations *kset1*, *kset2*, and *kset3* using deterministic rate equations translate into a stationary (in a stochastic sense [54]) regime in the Brownian simulator. In addition, the values for the average populations in the deterministic calculations, for all three parametrization sets, are ∼10 to ∼250 times smaller from what is obtained in our Brownian simulations (data not shown). It is worth mentioning that the collapse of the three dynamical regimes generated from the MWR rate equations into a common, stochastic, stationary regime has been observed also when the method of Gillespie [11] is used or when Gaussian noise is added to the rate equation solver [21]. Stochastic, well-mixed simulators also generate population levels that are substantially different. In detail, only the population of species C is consistently above zero, whereas species A and B weakly oscillate around zero [21]. It appears that when stochasticity is introduced in the MWR network via well-mixed simulators, the system becomes highly sensitive to fluctuations, especially if low particle numbers are employed [25].

B. Information transfer

A possible explanation of the peculiar behavior of species A and its relation with A's "double coupling" within the MWR network comes from the analysis of the information transfer quantified by the transfer entropy [55] defined as

$$T_{Y\to X} = \sum p\left(X_{n+1}, X_n^{(k)}, Y_n^{(l)}\right) \log \frac{p\left(X_{n+1} \mid X_n^{(k)}, Y_n^{(l)}\right)}{p\left(X_{n+1} \mid X_n^{(k)}\right)}, \tag{2}$$

where X_n is the state of species X at time step n and $X_n^{(k)} \equiv (X_n, \ldots, X_{n-k+1})$. In our calculations we consider $k = l = 1$. The transfer entropy is a particular case of the conditional mutual information $I(X,Y|Z)$ [56–58]. The transfer entropy defined in Eq. (2) quantifies how much knowing the state of species Y at time step n reduces the uncertainty of the state of X at time step $n+1$, conditioned on X_n. The transfer entropy is nonnegative and it is equal to zero when past values of species Y have no influence in determining (reducing the uncertainty on) the state of species X in the immediate future [55,59–63].

We use transfer entropy to estimate both the amount and the direction of the information transfer in the MWR network as well as their dependence from the presence of inert crowders and from the container's volume. A number of interesting conclusions can be inferred from the analysis of the transfer entropy data. Considering first the chemical network as a whole, the varying container volume does not significantly affect the information transfer between the different species in the network (variations are less than 0.5 bits—data not shown). For systems with a variable number of inert crowders (Fig. 4) there is a small but noticeable systematic increase in the transfer entropy with differences between the less and the most crowded systems of the order of 1 bit. A further look at the behavior of the single species shows the pivotal role of species A as a common *influencer* of the dynamics of species B and C. Indeed, Fig. 4 shows that the amount of information transferred from species A is systematically larger than the information transferred to species A in crowding number-varying systems. (The same result has been observed for variable volume, data not shown.) This asymmetry in the information (common to all three parametrization sets *kset1*, *kset2*, and *kset3*—*kset1* and *kset2* data not shown) can be linked to an increased ability of A to "absorb" external perturbations and therefore to its lower sensitivity to parameter change (see previous section).

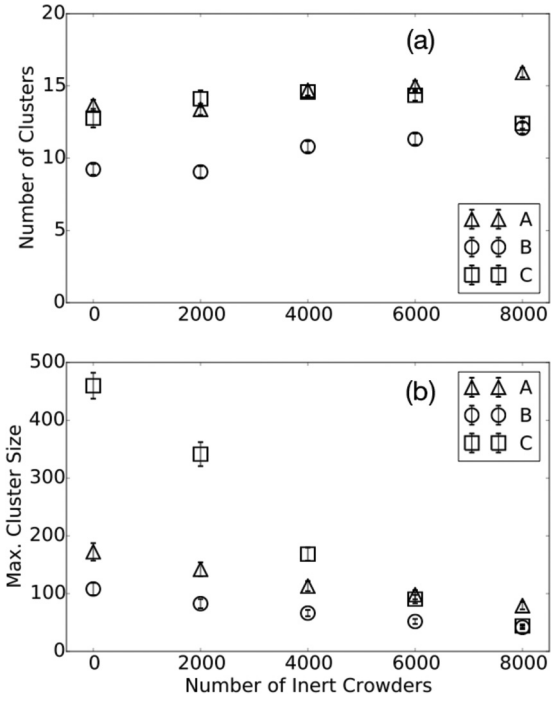

FIG. 6. Average number of clusters (a) and average maximum cluster size (b) as a function of the number of inert clusters. Data refer to species A, B, and C under *kset3* parametrization. The average number of clusters shows a weak tendency to increase for all three chemical species. The average maximum cluster size decreases with denser crowding conditions. The maximum cluster size in species C displays the largest decrease rate.

C. Statistical complexity

In this section we focus only on simulations performed under parametrization set *kset3* as this set of parameters appears to have an additional layer of complexity with respect to *kset1* and *kset2* and carries all the significant information

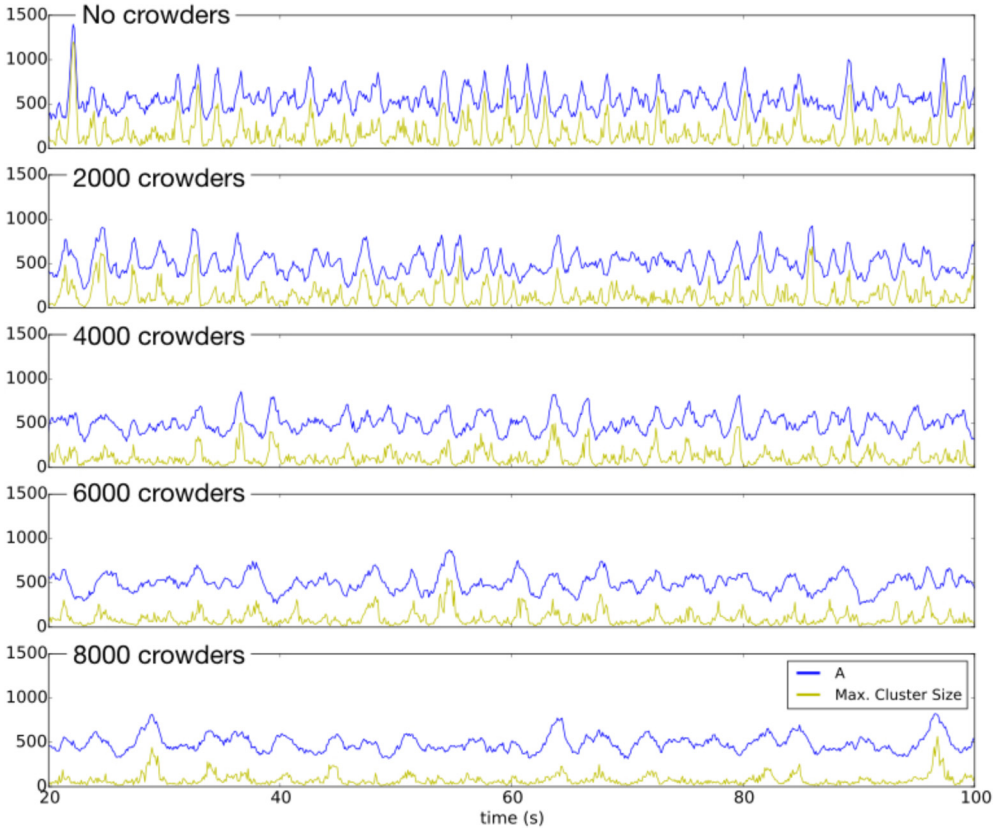

FIG. 7. Time evolution for the population size (blue) and the maximum cluster size (yellow). The temporal pattern in the maximum cluster size accurately mirrors the population size. Data refer to species A under *kset3* parametrization. The mutual information between the two sets of temporal data decreases with increasing number of crowders (see Table I).

about our system. IT functionals can be also used to estimate the degree of complexity in the time evolution of the chemical network and its dependence from the container volume and from the presence of inert crowders. The complexity estimation quantity that we choose is an intensive statistical complexity measure which is the product of the normalized spectral entropy $\hat{S}(P_r)$ and the intensive Jensen-Shannon divergence $\hat{Q}(P_r, P_e)$ [64,65] defined, respectively, as

$$\hat{S}(P_r) = -S_0 \sum_{r'}^{N_f} P_{r'} \log_2 P_{r'}, \tag{3}$$

with

$$P_r = \frac{f_r^2}{\sum_{r'}^{N_f} f_{r'}^2}, \tag{4}$$

where f_r are the frequencies in the Fourier spectrum and $N_f = 4000$ is the number of frequencies considered, and

$$\hat{Q}(P_r, P_e) = Q_0 \left[S\left(\frac{P_r + P_e}{2}\right) - \frac{1}{2} S(P_e) - \frac{1}{2} S(P_r) \right], \tag{5}$$

where $S(P_e) = \log_2 N_f = S_0^{-1}$, Q_0 is the normalization factor for Q, and $P_e = 1/N_f$.

The statistical complexity $\hat{S}\hat{Q}$ is zero for both $P_r = \{1,0,0,\ldots,0\}$ and $P_r = P_e = 1/N_f$, i.e., for spectral entropy $S = 0$ and $S = \log_2 N_f$ (fully ordered and fully stochastic systems) [65]. The results for the statistical complexity $\hat{S}\hat{Q}$ are shown in Fig. 5. Figure 5(a) shows that container volume variability does not significantly affect the average statistical complexity for species A, B, and C (both $\hat{S}$ and $\hat{Q}$ do not vary significantly; $\Delta \leqslant 0.02$). Conversely, for systems with constant volume and variable crowders number [Fig. 5(b)] the statistical complexity decreases with an increasing number of crowders. In detail, the decrease is almost exclusively due to a decrease in the normalized spectral entropy from 0.62 to 0.55,0.61 to 0.54, and 0.58 to 0.50, for species A, B, and C, respectively. The intensive Jensen-Shannon divergence remains constant at around 0.39–0.40. As a general conclusion from our information theoretic analysis, we can state that the presence of a growing number of inert crowders drives the chemical network toward a lower degree of complexity which is possibly due to a more efficient information transfer (see Fig. 4) between the reactive chemical species.

D. Spatial organization

The spatial organization of the chemical species in the network is investigated under the framework of (spectral) graph theory [66,67]. In detail, for each time step in each of our Brownian dynamics runs we build three binary, symmetric adjacency matrices G_A, G_B, and G_C for the three unweighted, undirected graphs representing the spatial connectivity network for species A, B, and C, respectively and separately. Two points (diffusing hard spheres of the same species) are connected if their distance at a given time

TABLE I. Mutual information (in bits) between population size and largest cluster size time series for species A, B, and C and for different numbers of inert crowders. Largest mutual information values correspond to a stronger nonlinear time correlation between population size and the size of the largest spatial cluster.

Inert crowders	A	B	C
0	0.969	0.811	1.574
2000	0.893	0.643	1.359
4000	0.847	0.619	0.806
6000	0.611	0.583	0.735
8000	0.568	0.471	0.442

step is $\leqslant 0.06$ μm. By definition, each point (hard sphere) is connected with itself and the diagonal elements of the matrices are therefore all equal to one. We then consider another three adjacency matrices G^s_A, G^s_B, and G^s_C, for species A, B, and C, respectively, of the subgraphs composed only by the points which are directly connected to four or more other points (hard spheres) of the same chemical species. We discard the remaining points which have less than four direct connections to other points as noise. This procedure is similar to the characterization of the "core" points in the DBSCAN clustering algorithm [68]. In other words, our approach is akin to a DBSCAN calculation where only the deterministic part is considered and where the "boundary" points are discarded as noise (DBSCAN* in Ref. [69]). It is easy to show [66] that, given a binary, symmetric adjacency matrix G of dimension m, the matrix $G_{\rm full} = G^{m-1}$ (which we call full connectivity matrix), where the power is defined in a boolean space [70], has element $g_{ij} = 1$ if and only if there is a connectivity path between points i and j, i.e., if and only if i and j belong to the same spatial cluster. The matrix $G_{\rm full}$ is binary, symmetric, and its diagonal elements are all equal to one. In order to speed up the calculations of the full connectivity matrix ($m \sim 10^3$) we exploit the existence of a simple bound on the diameter of our graph [71] and hence reduce the the matrix power exponent from $\sim 10^3$ to 15–20. The eigenvalues of $G_{\rm full}$ are real and all $\geqslant 0$. The number and the magnitude of the strictly positive eigenvalues correspond to the number and the size of the spatial clusters in our system, respectively, as these are the *connected components* of the graphs represented by the adjacency matrices G_A, G_B, and G_C [66,67]. In Fig. 6 we show the average number of clusters (a) and the average size of the largest cluster (b) as a function of the number of inert crowders. On the one hand, the average number of clusters shows a weak tendency to increase with increasing number of crowders for all three chemical species. On the other hand, the average maximum cluster size decreases with denser crowding conditions. Among the three reactive species the maximum cluster size in species C displays both the largest values and the largest decrease rate. Figure 6 basically shows that the presence of an increasing number of crowders opposes the natural tendency of the reactive particles in our system to aggregate in well-defined regions of the available space. An interesting feature of the maximum cluster size temporal evolution is shown in Fig. 7. For small numbers of crowders the maximum cluster size for species A tightly mirrors the time evolution of the population of species A (species B and C show very similar behavior—data not shown). The "correlation" between population dynamics and maximum cluster dynamics weakens with increasing crowder numbers. Indeed, Table I shows that the mutual information [56] between population and maximum cluster dynamics decreases with increasing crowder numbers. Similarly to what we observed in our analysis of the population dynamics and information transfer, the influence of a variable numbers of crowders on the spatial organization is not homogeneous across the three species in the chemical network.

IV. CONCLUSIONS

In this study we investigate the dynamical behavior of a generic chemical network under spatial confinement and crowding. We observe that the presence of inert crowders affects in a nontrivial way the population dynamics of the reactive species in the network. The choice of using IT for most of our analysis is motivated by the fact that the MWR network is a generic chemical system and that the quantities resulting from our simulations are stochastic in nature. IT offers in this case the most general approach to study interspecies (directional) correlations and the system's complex dynamical behavior. The detailed analysis of the population dynamics of the MWR network under different confinement and crowding conditions presented in Sec. III represents an extensive example of the level of detail, not accessible to deterministic and stochastic well-mixed models, that can be resolved when spatial confinement and crowding are explicitly taken into account.

In conclusion, we try to make the case for the use of spatial stochastic simulations as an elective method to complement experiments and to improve our understanding of complex, reaction-diffusion systems where dynamics is both spatially confined and compartmentalized. The code used for our Brownian simulations is available on request.

ACKNOWLEDGMENTS

The authors would like to thank Linda Petzold, Zachary Frazier, Frank Alber, Marco J. Morelli, and Steve Plimpton for useful discussions and for the help with the testing of our Brownian simulator. This work has been supported by NIH Grant No. 1R01EB014877-01.

[1] H. Qian, J. Phys. Chem. B **110**, 15063 (2006).
[2] H. Qian, Annu. Rev. Phys. Chem. **58**, 113 (2007).
[3] F. Ritort, *Nonequilibrium Fluctuations in Small Systems: From Physics to Biology* (John Wiley and Sons, New York, 2008), Chap. 2, pp. 31–123.
[4] P. Stano and P. L. Luisi, Curr. Opin. Biotechnol. **24**, 633 (2013).
[5] A. D. McNaught and A. Wilkinson, *IUPAC. Compendium of Chemical Terminology*, 2nd ed. (Blackwell Scientific, Oxford, 1997).

[6] D. H. Lee, K. Severin, and M. R. Ghadiri, Curr. Opin. Chem. Biol. **1**, 491 (1997).
[7] Z. Dadon, N. Wagner, and G. Ashkenasy, Angew. Chem., Int. Ed. Engl. **47**, 6128 (2008).
[8] N. Virgo and T. Ikegami, in *Advances in Artificial Life - ECAL 2013 - Proceedings of the Twelfth European Conference on the Synthesis and Simulation of Living Systems*, edited by P. Lio, O Miglino, G. Nicosia, S. Nolfi, and M. Pavone (MIT Press, Cambridge Mass., 2013), pp. 240–247.
[9] W. Hordijk, J. Hein, and M. Steel, Entropy **12**, 1733 (2010).
[10] H. A. Johnson, Q. Rev. Biol. **62**, 141 (1987).
[11] D. T. Gillespie, J. Phys. Chem. **81**, 2340 (1977).
[12] A. P. Minton, Biopolymers **20**, 2093 (1981).
[13] A. P. Minton, Methods Enzymol. **295**, 127 (1998).
[14] K. Luby-Phelps, Int. Rev. Cytol. **192**, 189 (2000).
[15] R. J. Ellis, Trends Biochem. Sci. **26**, 597 (2001).
[16] A. P. Minton, J. Biol. Chem. **276**, 10577 (2001).
[17] K. Richter, M. Nessling, and P. Lichter, J. Cell. Sci. **120**, 1673 (2007).
[18] K. Richter, M. Nessling, and P. Lichter, Biochim. Biophys. Acta **1783**, 2100 (2008).
[19] K. D. Willamowski and O. Rossler, Z. Naturforsch. A **35**, 317 (1980).
[20] B. D. Aguda and B. L. Clarke, J. Chem. Phys. **89**, 7428 (1988).
[21] J. Guemez and M. A. Matias, Phys. Rev. E **48**, R2351 (1993).
[22] P. Geysermans and G. Nicolis, J. Chem. Phys. **99**, 8964 (1993).
[23] A. Goryachev and R. Kapral, Phys. Rev. Lett. **76**, 1619 (1996).
[24] F. Chavez and R. Kapral, Phys. Rev. E **65**, 056203 (2002).
[25] J. W. Stucki and R. Urbanczik, Z. Naturforsch. A **60**, 599 (2005).
[26] T. Ando and J. Skolnick, Proc. Natl. Acad. Sci. U.S.A. **107**, 18457 (2010).
[27] T. Ando and S. Jeffrey, *Proceedings of the International Conference of the Quantum Bio-Informatics IV*, Vol. 28 (Georgia Institute of Technology, World Scientific, Singapore, 2011), pp. 413–426.
[28] M. J. Morelli and P. R. ten Wolde, J. Chem. Phys. **129**, 054112 (2008).
[29] Z. Frazier and F. Alber, J. Comput. Biol. **19**, 606 (2012).
[30] J. A. Lotka, J. Chem. Phys. **14**, 271 (1910).
[31] J. A. Lotka, J. Am. Chem. Soc. **42**, 1595 (1920).
[32] V. Volterra, Nature (London) **118**, 558 (1926).
[33] J. W. Szostak, D. P. Bartel, and P. L. Luisi, Nature (London) **409**, 387 (2001).
[34] E. Szathmary, Nature (London) **433**, 469 (2005).
[35] P. L. Luisi, F. Ferri, and P. Stano, Naturwissenschaften **93**, 1 (2006).
[36] Edited by S. Rasmussen, M. A. Bedau, L. Chen, D. Deamer, D. C. Krakauer, N. H. Packard, and P. F. Stadler, *Protocells, Bridging Nonliving and Living Matter* (MIT Press, Cambridge, MA, 2008).
[37] P. Stano, Syst. Synth. Biol. **4**, 149 (2010).
[38] S. A. Kauffman, Life **1**, 34 (2011).
[39] J. Gollihar, M. Levy, and A. D. Ellington, Science **343**, 259 (2014).
[40] Y. Elani, R. V. Law, and O. Ces, Nat. Commun. **5**, 5305 (2014).
[41] A. E. Engelhart, K. P. Adamala, and J. W. Szostak, Nat. Chem. **8**, 448 (2016).
[42] J. J. Tyson, K. C. Chen, and B. Novak, Curr. Opin. Cell Biol. **15**, 221 (2003).
[43] E. D. Herzog, Nat. Rev. Neurosci. **8**, 790 (2007).
[44] M. H. Jensen, S. Krishna, and S. Pigolotti, Phys. Rev. Lett. **103**, 118101 (2009).
[45] T. Danino, O. Mondragón-Palomino, L. Tsimring, and J. Hasty, Nature (London) **463**, 326 (2010).
[46] D. Ridgway, G. Broderick, A. Lopez-Campistrous, M. Ru'aini, P. Winter, M. Hamilton, P. Boulanger, A. Kovalenko, and M. J. Ellison, Biophys. J. **94**, 3748 (2008).
[47] J. S. Kim and A. Yethiraj, Biophys. J. **96**, 1333 (2009).
[48] J. S. Kim and A. Yethiraj, Biophys. J. **98**, 951 (2010).
[49] J. S. Kim and A. Yethiraj, J. Phys. Chem. B **115**, 347 (2011).
[50] G. Kwon, B. J. Sung, and A. Yethiraj, J. Phys. Chem. B **118**, 8128 (2014).
[51] M. Beck, M. Topf, Z. Frazier, H. Tjong, M. Xu, S. Zhang, and F. Alber, J. Struct. Biol. **173**, 483 (2011).
[52] D. T. Gillespie, A. Hellander, and L. Petzold, J. Chem. Phys. **138**, 170901 (2013).
[53] O. S. Andersen, J. Gen. Physiol. **125**, 3 (2005).
[54] N. G. Van Kampen, *Stochastic Processes in Physics and Chemistry*, 3rd ed. (Elsevier, Amsterdam, 2007).
[55] T. Schreiber, Phys. Rev. Lett. **85**, 461 (2000).
[56] T. M. Cover and J. A. Thomas, *Elements of Information Theory*, 2nd ed. (Wiley-Interscience, Hoboken, NJ, 2006).
[57] K. Hlavackova-Schindler, M. Palus, M. Vejmelka, and J. Bhattacharya, Phys. Rep. **441**, 1 (2007).
[58] M. Vejmelka and M. Palus, Phys. Rev. E **77**, 026214 (2008).
[59] J. T. Lizier and M. Prokopenko, Eur. Phys. J. B **73**, 605 (2010).
[60] M. Prokopenko, J. T. Lizier, and D. C. Price, Entropy **15**, 524 (2013).
[61] G. Ver Steeg, Non-Parametric Entropy Estimation Toolbox (NPEET) (2014), http://github.com/gregversteeg/NPEET.
[62] G. Ver Steeg and A. Galstyan, *Proceedings of the Sixth ACM International Conference on Web Search and Data Mining*, WSDM '13 (ACM, New York, 2013), pp. 3–12.
[63] A. Kraskov, H. Stogbauer, and P. Grassberger, Phys. Rev. E **69**, 066138 (2004).
[64] G. E. Powell and I. C. Percival, J. Phys. A **12**, 2053 (1979).
[65] O. A. Rosso, H. A. Larrondo, M. T. Martin, A. Plastino, and M. A. Fuentes, Phys. Rev. Lett. **99**, 154102 (2007).
[66] G. Chartrand, *Introductory Graph Theory* (Dover, New York, 1977).
[67] A. E. Brouwer and W. H. Haemers, *Spectra of Graphs* (Springer, Berlin, 2011).
[68] M. Ester, H.-P. Kriegel, J. Sander, and X. Xiaowei, in *Proceedings of the Second International Conference on Knowledge Discovery and Data Mining (KDD-96)*, edited by E. Simoudis, J. Han, and U. M. Fayyad (AAAI Press, Palo Alto CA, 1996), pp. 226–231.
[69] R. J. Campello, D. Moulavi, and J. Sander, *Advances in Knowledge Discovery and Data Mining* (Springer, Berlin, 2013), pp. 160–172.
[70] B. De Schutter and B. De Moor, SIAM J. Matrix Anal. Appl. **21**, 328 (1999).
[71] J. Kelner, *18.409 Topics in Theoretical Computer Science: An Algorithmist's Toolkit*, Fall 2009, Massachusetts Institute of Technology: MIT OpenCourseWare, https://ocw.mit.edu.